

Journal Article

A combined time-resolved infrared and density functional theory study of the lowest excited states of 9-fluorenone and 2-naphthaldehyde

Hanson-Heine, M.W.D., Calladine, J.A., Yang, J., Towrie, M., Hovarth, R., Besley, N.A., George, M.W

This article is published by Elsevier. The definitive version of this article is available at:

<https://www.sciencedirect.com/science/article/pii/S0012365X13005098>

Recommended citation:

Hanson-Heine, M.W.D., Calladine, J.A., Yang, J., Towrie, M., Hovarth, R., Besley, N.A., George, M.W (2018), *A combined time-resolved infrared and density functional theory study of the lowest excited states of 9-fluorenone and 2-naphthaldehyde*, In Press, Chemical Physics. Available online 24th April 2018. doi:
<https://doi.org/10.1016/j.chemphys.2018.04.014>

To be published in Chemical Physics in 2018

A combined time-resolved infrared and density functional theory study of the lowest excited states of 9-fluorenone and 2-naphthaldehyde

Magnus W.D. Hanson-Heine^a, James A. Calladine^a, Jixin Yang^a, Michael Towrie^b, Raphael Horvath^a, Nicholas A. Besley^{a,*}, Michael W. George^{a,c,*}

^a School of Chemistry, University of Nottingham, University Park, Nottingham NG7 2RD, UK

^b Central Laser Facility, Science & Technology Facilities Council, Research Complex at Harwell, Rutherford Appleton Laboratory, Didcot OX11 0QX, UK

^c Department of Chemical and Environmental Engineering, University of Nottingham Ningbo China, 199 Taikang East Road, Ningbo 315100, China

Abstract

A combined experimental and theoretical study of the infrared (IR) spectra of 2-naphthaldehyde and 9-fluorenone in their ground and first excited singlet and triplet electronic states is presented. IR studies have also been carried out using supercritical krypton (scKr) as a solvent to measure spectra in the ground and triplet excited states. This solvent provides a weakly interacting environment that is closer to the gas phase and allows a direct comparison with the calculated spectra for a single molecule. The IR spectra for the three different states are computed with Kohn-Sham density functional theory. For the first excited singlet state it is necessary to use an overlap procedure that allows the excited state to be studied by preventing variational collapse to the ground state. This allows the excited singlet state to be studied in an analogous approach to the ground and excited triplet state, in contrast to using time dependent density functional theory. The good agreement between the calculated excited state spectra and the experiment provides insight into the nature of the excited states. For the ground and excited triplet state the anharmonic vibrational frequencies are computed using the transition optimized shifted Hermite method, and for these molecules the hybrid B97-1 functional is found to provide the closest agreement with experiment in the ground state.

1. Introduction

Time-resolved infrared spectroscopy (TRIR), a combination of UV flash photolysis and very fast IR spectroscopy, has proven to be a successful and effective technique for characterizing molecules in their electronically excited states [1–6]. The combination of TRIR with quantum chemical calculations can provide detailed insights into the electronic structure as well providing a mechanism to assess the accuracy of quantum chemical methods. Calculations of IR spectra are usually based upon the harmonic approximation. These calculations can provide band assignments, and for excited state spectra the nature of the excited state can be identified provided that a sufficiently good match exists between the ground and excited state experimental and calculated spectra [7,8].

The study of the IR spectroscopy of electronically excited states presents additional challenges to theory. Quantum chemical methods that are able to study electronically excited states are usually less accurate than their ground state counterparts and the vibrational modes themselves can become increasingly delocalized [9]. The study of lowest triplet excited states provides an interesting intermediate case where the vibrational modes of an electronically excited state can be studied with formally ground state electronic structure methods whereas to study the first excited singlet state requires a 'genuine' excited state method to be used. In comparison to calculations of the IR spectra of molecules in their ground states, there have been fewer computational studies of electronic singlet excited state spectra. This is in part due to the additional complexity of computing these spectra but also to the lack of reliable experimental data for larger molecules in the gas-phase.

The nature of electronically excited states means that anharmonic effects may become increasingly significant. The inclusion of anharmonic effects to calculate IR spectra requires higher order derivatives of the nuclear potential energy surface to be determined. This rapidly becomes prohibitive as the size of the molecule increases owing to the associated computational cost. However, the continued development of both computer resources and computational methodology has made more rigorous treatments of anharmonicity possible for increasingly larger molecules [10–18]. Despite these advances, the computation of anharmonic frequencies remains uncommon, and usually harmonic frequencies are computed and empirical scaling factors used [19–25]. These scaling factors will correct the frequencies for anharmonicity but will also incorporate corrections for the underlying electronic structure method. In some cases it is not necessary to scale the harmonic frequencies [26,27], which will clearly rely on a subtle balance between errors in the harmonic energy surface and the electronic structure methods used, and indeed the production of a density functional theory (DFT) functional parameterized using harmonic frequencies did not seem to produce optimum results [28]. Consequently it is desirable to be able to compute accurate anharmonic frequencies where possible since this provides a more valid test of the electronic structure method.

Aromatic carbonyls are known to possess two low-lying excited states of $n\pi^*$ and $\pi\pi^*$ character in both the triplet and singlet manifolds, and the relative energy of these states is sensitive to changes in the substituent and solvation environments [29]. Consequently aromatic carbonyls are regularly used as a prototype molecule for studying photochemical processes, and assignment of their lowest triplet and singlet states is of significant interest with studies combining TRIR, time-resolved resonance Raman [30], and DFT being reported in a wide variety of polar and non-polar solvents for molecules including benzophenone [31,32], decafluorobenzophenone [33], 4-phenylbenzophenone [34], 9-fluorenone [35–38], and 2-naphthaldehyde [39–41], to name but a few.

In this paper we present a combined experimental and computational study of the IR spectroscopy of the ground and first excited singlet and triplet states of 2-naphthaldehyde and 9-fluorenone. TRIR spectra are recorded in deuterated acetonitrile (T_1 and S_1 states) and supercritical krypton (scKr) (S_0 and T_1 states) solvents and compared with spectra calculated using DFT with the harmonic approximation. The calculations allow the nature of the excited states to be determined. For the ground state and T_1 excited state, anharmonic frequencies are also evaluated using the transition optimized shifted Hermite (TOSH) method [42]. Recent studies have shown that the optimal DFT theory is sensitive to the frequencies under investigation [43], and we investigate the performance of some widely used hybrid and gradient-corrected DFT exchange-correlation functionals, namely B3LYP [44,45], BLYP [46,47], EDF1 [48], EDF2 [28], B97-1 [49], and B97-2 [50], for ground state data in supercritical krypton (scKr).

2. Experimental details

All compounds were used as supplied (from Aldrich). IR spectra of supercritical fluid solutions were measured in a custom-built high pressure cell, designed for pressures up to 5000 psi. The step-scan FTIR (s^2 -FTIR) experiments were conducted using a combination of a Nicolet Magna 860 Interferometer and a Nd:YAG laser (Spectra Physics GCR12) [51]. Synchronization of the laser with data collection was achieved using a pulse generator (Stanford DG535). The interferometer was equipped with both an internal 100 kHz 16-bit digitizer and an external 100 MHz 12-bit digitiser (GAGE 8012A). In these experiments a 1 mm photovoltaic MCT detector was used with a 50 MHz preamplifier. This detector has AC and DC outputs, which are digitised simultaneously to ensure proper phase matching. The AC signal was amplified by an external preamplifier (Stanford SR 560) to use the full dynamic range of the digitizer. Single sided interferograms were obtained using one laser pulse at each mirror position. An external optical bench (Nicolet-TOM[®]) was used for locating the sample cell and MCT detector, allowing easy manipulation of the UV laser beam through the cell. All s^2 -FTIR spectra reported in this paper were recorded at 8 cm^{-1} resolution with 64 scans of the interferometer using a supercritical fluid flow system and 4-port cell which has been described in detail elsewhere [52].

Ultrafast TRIR spectroscopic experiments in deuterated acetonitrile solution was carried out using the ULTRA facility [53] located at the Rutherford Appleton Laboratory, using time-resolved multiple probe spectroscopy (TR^MPS) and a detailed description of this instrument has been published previously [53]. Briefly, the TR^MPS experiment utilizes a pump-probe-probe-probe recording scheme afforded by synchronizing two oscillators. The pump laser is tuned to 355 nm by optical parametric amplification (OPA) while the mid-IR probe is generated using OPAs with difference-frequency mixing units. The pump-probe delay is controlled using a combination of electronic and optical delays, which allows time-delays from picoseconds to milliseconds to be achieved in a single experiment. The pump pulse was set to ca. 2 mJ/pulse at the sample using a neutral density filter. Pump and probe beam polarizations were set at the magic angle. A portion of the probe beam was dispersed onto an MCT detector as a reference, while the remainder was passed through the sample, dispersed by grating monochromators and detected by two 128-channel linear array MCT detectors.

3. Computational details

Geometry optimizations and frequency calculations were performed with Kohn-Sham DFT in combination with the B3LYP, BLYP, EDF1, EDF2, B97-1, and B97-2 exchange–correlation functionals and 6-311G(d,p) basis set using the Q-Chem quantum-chemical software package [54]. The 6-311G(d,p) basis set was chosen since it represents a good compromise between accuracy and computational cost. Initial molecular structures were optimized to minimum energy geometries at each level of theory, before the calculation of vibrational frequencies and intensities. The triplet excited state was studied using unrestricted DFT while the maximum overlap method (MOM) [55] was used to allow the excited singlet state to be computed. In this approach, the open-shell excited singlet is described by a single determinant which gives a spin-mixed state. In the calculations presented here, a spin-purified form is used wherein the energy of the excited singlet state is expressed as $E = 2E_S - E_T$, where E_S and E_T are the single determinant singlet state energy and the energy of the corresponding triplet state, respectively. Previous work has demonstrated that IR spectra for excited singlet states calculated with this approach are in good agreement with experiment [7,9].

Harmonic vibrational frequencies and normal modes were determined using analytic second derivatives of the energy with respect to nuclear displacement. Anharmonic corrections to

the vibrational frequencies were computed using the TOSH method based upon the quartic force field with up to two-mode coupling terms [42]. The third- and fourth-order derivatives of the energy with respect to the nuclear displacements were evaluated numerically from finite differences of the analytic energy, gradient, and Hessian, using the default step size of $0.1 a_0$ [42].

Simulated spectra for the frequency range 1200 and 1800 cm^{-1} have been generated by representing each vibrational band as a Gaussian function with an area proportional to its calculated intensity, and a bandwidth determined by that intensity. Gaussian bandwidths of 2, 3, 4, 5, and 6 cm^{-1} were used for intensities in the ranges <10, 10–20, 20–30, 30–150, and >150 km mol^{-1} respectively, as these assignments were previously found to give the best visual agreement with the experimental data [55]. Functional specific harmonic frequency scaling factors proposed by Merrick *et al.* for the 6-311+G(d,p) basis set were used [21]. The scaling factors 0.9688, 0.9684, 0.9587, and 0.9668 were used to scale the B3LYP, B97-1, B97-2, and EDF2 hybrid functionals, respectively. Harmonic normal mode displacement vectors were visualised using the VMD software package [56].

4. Results and discussion

4.1. Ground state

Before considering the excited states we will examine the ground state. The simulated spectra based upon the harmonic frequencies for the ground states of 9-fluorenone and 2-naphthaldehyde along with the FTIR spectra recorded in scKr are shown in Fig. 1 with the calculated and experimental vibrational frequencies summarized in Tables 1 and 2. As mentioned above we have used the supercritical noble gas solvent since it is expected to closely represent the simulations carried out in vacuo allowing a direct comparison to be made. The calculated spectra in Fig. 1 are based upon calculations using the EDF1 exchange-correlation functional. As noted in previous studies [26,43], harmonic frequencies computed using EDF1 are close to experiment and scaling of the frequencies is not required. Mean absolute deviations (MADs) between the experimental and calculated frequencies for the 1200 and 1800 cm^{-1} frequency range are shown in Figs. 2 and 3. For the EDF1 functional, MADs of 10 cm^{-1} and 4 cm^{-1} are obtained for 2-naphthaldehyde and 9-fluorenone, respectively. This represents a very good level of agreement and this functional is also noteworthy in that it gives accurate frequencies for the carbonyl stretching modes. These computed frequencies result in simulated spectra that closely resemble the experimental spectra for both molecules.

As expected, the hybrid functionals systematically overestimate the experimental frequencies, on average by between ca. 30 to 50 cm^{-1} , as they do not benefit from the same cancellation of errors. For the other functionals, scaling the harmonic frequencies reduces the deviation from experiment. The best results for scaling were found for the B3LYP functional, with the MAD falling from 34 to 18 cm^{-1} . Here we note that the scaled frequencies tend to underestimate the experimental frequencies, and the resulting MAD is greater than for the EDF1 functional.

Normal mode displacements for the EDF1 calculations are illustrated in Tables 1 and 2 for the vibrational modes that correspond to bands observed in experiment. The highest frequency modes of 1715 cm^{-1} in 2-naphthaldehyde and 1732 cm^{-1} in 9-fluorenone, in the experimental data with scKr solvent, are localized on the carbonyl group and correspond to the carbonyl stretching mode. The remaining modes contain a high degree of out-of-phase ring carbon stretching and in-phase ring carbon displacements. The band arising from the

carbonyl stretching mode is the most intense band observed in the spectra and is of particular importance since the shift of this band can be used as a diagnostic of the nature of an excited state. The experimental data shows that this band is sensitive to the environment, with shifts of -14 cm^{-1} and -19 cm^{-1} for 9-fluorenone and 2-naphthaldehyde in CD_3CN solvent compared with scKr. In comparison the other vibrational modes differ by less than 5 cm^{-1} . A closer examination of the frequency of the carbonyl stretching mode shows that its frequency is 17 cm^{-1} higher in 9-fluorenone compared with 2-naphthaldehyde. The EDF1 calculations underestimate this separation and predict a difference of 5 cm^{-1} between the two molecules. The B97-1 functional finds a difference of 12 cm^{-1} , which is closer to experiment. Consequently, even though the EDF1 functional has a significantly lower MAD, its quantitative prediction in this regard is worse than B97-1 illustrating that MAD values can be insensitive to more subtle comparisons.

4.2. S_1 and T_1 excited states

The IR spectra for the T_1 and S_1 states of 2-naphthaldehyde are shown in Figs. 4 and 5 together with the TRIR traces in Fig. 6, showing the decay of the S_1 to the T_1 state. The vibrational frequencies of the prominent features listed are in Table 3. The spectra for T_1 state are dominated by bands at about 1600 cm^{-1} , with the remaining bands weak in comparison. The triplet excited state spectra were acquired 100 ns (in CD_3CN) and 1 μs (in scKr) after photoexcitation with a 355 nm pulse [57]. After photoexcitation, bleaching of the parent bands is evident, and new T_1 $\nu(\text{CO})$ bands at 1600 cm^{-1} and 1626 cm^{-1} for CD_3CN and scKr respectively, appear. These band positions are similar to the 1620 cm^{-1} band reported in a previous study in cyclohexane of 1620 cm^{-1} for the T_1 state [57]. This represents a shift of ca. 90 cm^{-1} , with the frequency of the $\nu(\text{CO})$ band sensitive to the polarity of the solvent. Previous work has identified an increased solvent-solute interaction when examining the similar $\pi\pi^*$ states of 9-fluorenone in polar solvents [36,58]. A second peak in the CO region at ca. 1591 cm^{-1} is observed in CD_3CN but not in scKr. The calculations (see later) show no evidence of a peak in this region and definitive assignment of this band is not possible. However, one possibility is that this extra band is due to some form of aggregation *i.e.* dimerization that occurs at higher concentrations used in the experiments carried out in CD_3CN compared to scKr or the presence of a rotational conformer formed by rotation of the aldehyde group due to changes in the electronic structure following photo-excitation. For the S_1 state, recorded spectra are only available for CD_3CN solvent. The $\nu(\text{CO})$ band is observed at 1638 cm^{-1} , with a corresponding value of 1600 cm^{-1} for the T_1 state. This shows that the carbonyl bond is weakened more in the T_1 state compared with the S_1 state. Another notable difference of the S_1 state spectra is a prominent band at 1300 cm^{-1} which corresponds to in-plane wagging of the hydrogen atoms (see Table 4).

For 9-fluorenone the IR spectra for the T_1 and S_1 states are shown in Figs. 7 and 8 with the TRIR traces in Fig. 9. Similar to 2-naphthaldehyde, the spectra also have an intense band in the region of 1600 cm^{-1} which arises from the carbonyl stretching mode. However, for 9-fluorenone more distinct bands can be distinguished at lower frequencies. For the T_1 state the $\nu(\text{CO})$ band is observed at 1596 cm^{-1} in CD_3CN and 1616 cm^{-1} in scKr. This represents shifts of 122 cm^{-1} and 116 cm^{-1} , which are larger than the corresponding shifts in 2-naphthaldehyde. Previously observed peaks at 1600, 1544 and 1480 cm^{-1} in CD_3CN are in good agreement with our data. For the S_1 state the $\nu(\text{CO})$ band is observed at 1545 cm^{-1} . This represents a significance difference to 2-naphthaldehyde. In 2-naphthaldehyde the frequency of the $\nu(\text{CO})$ band is greater in the S_1 state (by 38 cm^{-1}) whereas in 9-fluorenone the frequency in the S_1 state is lower (by 51 cm^{-1}).

The orbitals involved in the lowest electronic excitations for 9-fluorenone and 2-naphthaldehyde are shown in Figs. 10 and 11. The highest occupied molecular orbitals (HOMOs) have π -orbital character and are localized on the aromatic rings of the two systems, while the lowest unoccupied molecular orbitals (LUMOs) are of π^* -orbital (anti-bonding) character and are also localized on the rings. Both molecules also have a non-bonding HOMO-1 orbital localized on the carbonyl oxygen atom. These orbitals show that the states arising from the HOMO to LUMO transition can be described as $\pi\pi^*$ in vacuo, consistent with experimental results [57,59,60].

The calculated spectra for the T_1 and S_1 excited states are shown in Figs. 4 and 5 for 2-naphthaldehyde and Figs. 7 and 8 for 9-fluorenone. The spectra have been calculated with the B97-1 functional in combination with the 6-311G(d,p) basis set with the frequencies scaled by 0.9688. For the excited states, it was not possible to converge the EDF1 calculation for the triplet state to a satisfactory level, and the high level of accuracy observed for the ground state was not obtained. First we consider 2-naphthaldehyde. For both the T_1 and S_1 states, the calculations reproduce the features of the experimental spectra. The most intense peak in the spectra corresponds to the carbonyl stretching mode that is shifted by -112 cm^{-1} for the T_1 state and -106 cm^{-1} for the S_1 state relative to the corresponding ground state calculation. The magnitude of this shift is similar to the value observed in experiment and is associated with a weakening of the C=O bond as a result of exciting an electron to an orbital that is anti-bonding (has a node) character along this bond, and confirms the assignment of these states as $\pi\pi^*$. The weaker bands also occur at frequencies in regions where peaks can be distinguished in the experimental spectra (shown in Table 3). The main discrepancy between the calculated spectra and experiment is the predicted frequency of the carbonyl stretching mode in the S_1 state is too low and this results in a difference in frequency of this band between the T_1 and S_1 states of only 6 cm^{-1} compared with a value of 38 cm^{-1} in experiment, however the calculations do correctly predict a higher frequency for the S_1 state.

The calculated spectra for 9-fluorenone also show a large shift in the carbonyl stretching mode characteristic of $\pi\pi^*$ states. The frequencies of these modes are 1565 cm^{-1} and 1603 cm^{-1} for the S_1 and T_1 states, compared with values of 1545 and 1596 cm^{-1} in experiment. The main difference between the calculated and experimental spectra is associated with the intensities of the bands that lie below the carbonyl stretching mode. Bands in this region of the spectrum can be clearly identified in experiment, but the calculations predict the bands to have much greater intensity relative to the carbonyl band and this occurs for both the triplet and singlet states. Relative intensity differences can arise from the double harmonic approximation used to calculate simulated IR intensities, and these values may be more susceptible to basis set or other deficiencies in the excited state method. The spin-purification treatment of the singlet excited state used here, incorporates the energy of the triplet state. Consequently, any error in the description of the triplet state will be inherited by the singlet state calculation. The T_1 state of 9-fluorenone appears to be a challenge for the methodology used here, as discussed above this state could not be described correctly by the EDF1 functional, and may indicate that this state has multi-determinant character and is not well described by a single determinant that underlies the calculations presented.

5. Anharmonic frequency calculations

Anharmonic frequencies were computed for the ground and T_1 state using the B97-1 functional. This analysis is not performed for the S_1 state owing to technical difficulties in extending the spin purified MOM approach to compute all of the derivatives necessary for anharmonic frequency calculations. The computed frequencies for the ground state are given in Tables 1 and 2, with MADs shown in Figs. 12 and 13. Overall, the B97-1 functional

gives the best performance, with the B3LYP functional also performing well. This is consistent with previous studies that have identified these functionals as being reliable for anharmonic frequency calculations [27]. The calculated anharmonic frequencies significantly improve the unscaled harmonic frequencies. For most of the vibrational modes the calculations underestimate the anharmonic correction, resulting in frequencies that are too high. The exception to this is the carbonyl stretching mode in 9-fluorenone. For this mode the anharmonic calculation appears to fail and does not improve the frequency. Identifying the precise reasons for this failure is difficult, but it may be related to some numerical instability in the calculations. The B97-1 calculations were extended to the T_1 state and the computed frequencies for the vibrational modes observed in experiment are shown in Tables 5 and 6. The resulting frequencies are in good agreement with the experimental data with most of the vibrational modes predicted within 10 cm^{-1} of the experimental values in scKr.

6. Conclusions

Ground state infrared spectra recorded in deuterated acetonitrile and super critical krypton solvents have been compared with DFT calculations. The experimental data shows that the most intense band in the 1200 and 1800 cm^{-1} frequency range, which corresponds to the carbonyl stretching mode, is sensitive to the solvent environment. Simulated spectra based upon harmonic frequencies computed with the EDF1 exchange-correlation functional reproduce the experimental spectra well and allow the observed bands to be assigned to vibrational modes. Anharmonic vibrational frequencies calculated with the TOSH method using a selection of exchange-correlation functionals, find the B97-1 functional to perform best. The mean absolute deviations between the prominent vibrational peaks in the spectral window between 1200 and 1800 cm^{-1} show good matches between calculation and experiment for 9-fluorenone and 2-naphthaldehyde, with the exception of the carbonyl stretching mode of 9-fluorenone.

Excited state TRIR spectra are also reported for the T_1 and S_1 states of 9-fluorenone and 2-naphthaldehyde. The experimental spectra show a shift of between 90 and 120 cm^{-1} in the carbonyl stretching mode in the excited states. The experimental data shows the frequency of the $\nu(\text{CO})$ band to be larger in the S_1 state compared with the T_1 state for 2-naphthaldehyde, while for 9-fluorenone the frequency is higher in the T_1 state. The DFT calculations show these states to be $\pi\pi^*$ states. The spectra computed for these states provide a qualitatively correct description of the experimental data and correctly identify the shift in the carbonyl band to be larger for the S_1 state in 9-fluorenone but larger for the T_1 state in 2-naphthaldehyde. The calculated anharmonic frequencies for the T_1 state are in good agreement with experiment with most of the vibrational modes predicted within 10 cm^{-1} of the experimental values in scKr. Overall, the work demonstrates that Kohn-Sham DFT based calculations of excited state IR spectra for low lying excited states can be used successfully to identify the nature of the excited state and interpret experimental spectra.

Acknowledgments

This work was supported by the Engineering and Physical Sciences Research Council [Grant No. EP/N002148/1]. The authors would like to thank the University of Nottingham for access to its High Performance Computing facility.

References

- [1] M.W. George, M. Poliakoff, J.J. Turner, *Analyst*. 119 (4) (1994) 551–560.
- [2] P. Glyn, M.W. George, P.M. Hodges, J.J. Turner, *J. Chem. Soc. Chem. Commun.* 21 (1989) 1655–1657.
- [3] M.W. George, C. Kato, H. Hamaguchi, *Chem. Lett.* 5 (1993) 873–876.
- [4] J.P. Toscano, in: *Advances in Photochemistry*, John Wiley & Sons, Inc., 2007, pp. 41–91.
- [5] R. Horvath, G.S. Huff, K.C. Gordon, M.W. George, *Coord. Chem. Rev.* 325 (2016) 41–58.
- [6] a) Q.C. Sun, B. Dereka, E. Vauthey, L.M.L. Daku, A. Hauser, *Chem. Sci.* 8(1) (2017) 223–230. b) M. Abdellah, A.M. El-Zohry, L.J. Antila, C.D. Windle, E. Reisner, L. Hammarstrom, *J. Am. Chem. Soc.* 139(3) (2017) 1226–1232. c) N.T. La Porte, J.F. Martinez, S. Hedstrom, B. Rudshteyn, B.T. Phelan, C.M. Mauck, R.M. Young, V.S. Batista, M.R. Wasielewski, *Chem. Sci.* 8(5) (2017) 3821–3831. d) T.J. Reade, T.S. Murphy, J.A. Calladine, R. Horvath, I.P. Clark, G.M. Greetham, M. Towrie, W. Lewis, M.W. George, N.R. Champness, *Phil. Trans. R. Soc. A* 375 (2084) (2017). e) D.J. Heyes, S.J.O. Hardman, D. Mansell, A. Ni Cheallaigh, J.M. Gardiner, L.O. Johannissen, G.M. Greetham, M. Towrie, N. S. Scrutton, *J. Phys. Chem. B* 121(6) (2017) 1312–1320. f) M. Hada, S. Saito, S. Tanaka, R. Sato, M. Yoshimura, K. Mouri, K. Matsuo, S. Yamaguchi, M. Hara, Y. Hayashi, F. Rohricht, R. Herges, Y. Shigeta, K. Onda, R.J.D. Miller, *J. Am. Chem. Soc.* 139(44) (2017) 15792–15800. g) J. Torres-Alacan, P. Vohringer, *Chem. Eur. J.* 23(28) (2017) 6746–6751. h) J. Ahrens, M. Frank, G.H. Clever, D. Schwarzer, *Phys. Chem. Chem. Phys.* 19(21) (2017) 13596–13603. i) T. Mukuta, P.V. Simpson, J.G. Vaughan, B.W. Skelton, S. Stagni, M. Massi, K. Koike, O. Ishitani, K. Onda, *Inorg. Chem.* 56(6) (2017) 3404–3413. j) B. Wezislá, J. Lindner, U. Das, A.C. Filippou, P. Vohringer, *Angew. Chem. Int. Ed.* 56(24) (2017) 6901–6905. k) M. Delor, S.A. Archer, T. Keane, A. Meijer, I.V. Sazanovich, G.M. Greetham, M. Towrie, J.A. Weinstein, *Nat. Chem.* 9(11) (2017) 1099–1104. l) J. Ojeda, C.A. Arrell, L. m) Longetti, M. Chergui, J. Helbing, *Phys. Chem. Chem. Phys.* 19(26) (2017) 17052–17062. n) C.C. Jiang, P.J. Young, S. Brown-Xu, J.C. Gallucci, M.H. Chisholm, *Inorg. Chem.* 56(3) (2017) 1433–1445. o) M. Zimmer, F. Dietrich, D. Volz, S. Brase, M. Gerhards, *ChemPhysChem* 18(21) (2017) 3023–3029. p) M. Pizl, B.M. Hunter, G.M. Greetham, M. Towrie, S. Zalis, H.B. Gray, A. Vlcek, *J. Phys. Chem. A* 121(48) (2017) 9275–9283. q) T. Suhina, S. Amirjalayer, S. Woutersen, D. Bonn, A.M. Brouwer, *Phys. Chem. Chem. Phys.* 19(30) (2017) 19998–20007. r) M. Di Donato, M.M. Lerch, A. Lapini, A.D. Laurent, A. Iagatti, L. Bussotti, S.P. Ihrig, M. Medved, D. Jacquemin, W. Szymanski, W.J. Buma, P. Foggi, B.L. Feringa, *J. Am. Chem. Soc.* 139(44) (2017) 15596–15599. s) C.M. Mauck, R.M. Young, M.R. Wasielewski, *J. Phys. Chem. A* 121(4) (2017) 784–792. t) F.A. Black, C.A. Clark, G.H. Summers, I.P. Clark, M. Towrie, T. Penfold, M.W. George, E.A. Gibson, *Phys. Chem. Chem. Phys.* 19(11) (2017) 7877–7885. u) P.A. Summers, J.A. Calladine, N. Ibrahim, K.P. Kusumo, C.A. Clark, X.Z. Sun, M.L. Hamilton, M. Towrie, J. McMaster, M. Schroder, M.W. George, *Polyhedron* 123 (2017) 259–264. v) B.S. Adams, G.E. Shillito, H. van der Salm, R. Horvath, C. B. Larsen, X.Z. Sun, N.T. Lucas, M.W. George, K.C. Gordon, *Inorg. Chem.* 56(21) (2017) 12967–12977. w) A.A. Gil, S.P. Laptanok, J.N. Iuliano, A. Lukacs, A. Verma, C.R. Hall, G.E. Yoon, R. Brust, G.M. Greetham, M. Towrie, J.B. French, S.R. Meech, P.J. Tonge, *J. Am. Chem. Soc.* 139(41) (2017) 14638–14648. x) C.J. Cardin, J.M. Kelly, S.J. Quinn, *Chem. Sci.* 8(7) (2017) 4705–4723.
- [7] M.W.D. Hanson-Heine, M.W. George, N.A. Besley, *J. Chem. Phys.* 138 (6) (2013) 064101.
- [8] M. Reinhard, G. Auböck, N.A. Besley, I.P. Clark, G.M. Greetham, M.W.D. Hanson-Heine, R. Horvath, T.S. Murphy, T.J. Penfold, M. Towrie, M.W. George, M.

- Chergui, J. Am. Chem. Soc. 139 (21) (2017) 7335–7347.
- [9] M.W.D. Hanson-Heine, A. Wriglesworth, M. Uroos, J.A. Calladine, T.S. Murphy, M. Hamilton, I.P. Clark, M. Towrie, J. Dowden, N.A. Besley, M.W. George, J. Chem. Phys. 142 (15) (2015) 154119.
- [10] A. Miani, E. Cane, P. Palmieri, A. Trombetti, N.C. Handy, J. Chem. Phys. 112 (1) (2000) 248–259.
- [11] V. Barone, J. Phys. Chem. A 108 (18) (2004) 4146–4150.
- [12] A.D. Boese, J.M.L. Martin, J. Phys. Chem. A 108 (15) (2004) 3085–3096.
- [13] E. Cane, A. Miani, A. Trombetti, J. Phys. Chem. A 111 (33) (2007) 8218–8222.
- [14] E. Cane, A. Trombetti, Phys. Chem. Chem. Phys. 11 (14) (2009) 2428–2432.
- [15] J. Dreyer, J. Chem. Phys. 127 (5) (2007) 054309.
- [16] X. Cheng, R.P. Steele, J. Chem. Phys. 141 (10) (2014) 104105.
- [17] M.W.D. Hanson-Heine, J. Chem. Phys. 143 (16) (2015) 164104.
- [18] M.W.D. Hanson-Heine, J. Chem. Phys. 144 (20) (2016) 204116.
- [19] A.P. Scott, L. Radom, J. Phys. Chem. 100 (41) (1996) 16502–16513.
- [20] M.P. Andersson, P. Uvdal, J. Phys. Chem. A 109 (12) (2005) 2937–2941.
- [21] J.P. Merrick, D. Moran, L. Radom, J. Phys. Chem. A 111 (45) (2007) 11683–11700.
- [22] Y. Tantirungrotechai, K. Phanasant, S. Roddecha, P. Surawatanawong, V. Sutthikhum, J. Limtrakul, J. Mol. Struct. (Theochem) 760 (1–3) (2006) 189–192.
- [23] M.W. Wong, Chem. Phys. Lett. 256 (4–5) (1996) 391–399.
- [24] D.J. Defrees, A.D. Mclean, J. Chem. Phys. 82 (1) (1985) 333–341.
- [25] J.A. Pople, A.P. Scott, M.W. Wong, L. Radom, Isr. J. Chem. 33 (3) (1993) 345–350.
- [26] T.M. Watson, J.D. Hirst, J. Phys. Chem. A 106 (34) (2002) 7858–7867.
- [27] M.W.D. Hanson-Heine, M.W. George, N.A. Besley, J. Phys. Chem. A 116 (17) (2012) 4417–4425.
- [28] C.Y. Lin, M.W. George, P.M.W. Gill, Aust. J. Chem. 57 (4) (2004) 365–370.
- [29] N.J. Turro, V. Ramamurthy, J.C. Scaiano, ChemPhysChem 12 (2011) 2496–2497.
- [30] S.K. Sahoo, S. Umapathy, A.W. Parker, Appl. Spectrosc. 65 (10) (2011) 1087–1115.
- [31] S. Dym, R.M. Hochstrasser, M. Schafer, J. Chem. Phys. 48 (1968) 646–652.
- [32] T. Tahara, H. Hamaguchi, M. Tasumi, J. Phys. Chem. 91 (1987) 5875–5880.
- [33] R. Anandhi, S. Umapathy, J. Raman Spectrosc. 31 (2000) 331–338.
- [34] T. Tahara, H. Hamaguchi, M. Tasumi, J. Phys. Chem. 94 (1990) 170–178.
- [35] S. Tanaka, C. Kato, K. Horie, H. Hamaguchi, Chem. Phys. Lett. 381 (2003) 385–391.
- [36] C. Sun, J. Liu, W.Z. Liang, Y. Zhao, Chin. J. Chem. Phys. 26 (6) (2013) 617–626.
- [37] R. Ghosh, A.K. Mora, S. Nath, D.K. Palit, J. Phys. Chem. B 121 (5) (2017) 1068–1080.
- [38] Y. Fukui, K. Ohta, K. Tominaga, Faraday Discuss. 177 (2015) 65–75.
- [39] A.M.J. Vaneijk, P.F.A. Verhey, A.H. Huizer, C. Varma, J. Am. Chem. Soc. 109 (22) (1987) 6635–6641.
- [40] A.M.J. Vaneijk, G.B. Ekelmans, R. Vandersteen, A.H. Huizer, C. Varma, Chem. Soc. Faraday Trans. 2 (84) (1988) 1129–1137.
- [41] M.J. Vanderburgt, A.H. Huizer, C. Varma, B.D. Wagner, J. Luszytk, Chem. Phys. 196 (1–2) (1995) 193–210.
- [42] C.Y. Lin, A.T.B. Gilbert, P.M.W. Gill, Theor. Chem. Acc. 120 (1–3) (2008) 23–35.
- [43] M.W.D. Hanson-Heine, M.W. George, N.A. Besley, J. Phys. Chem. A 116 (2012) 4417–4425.
- [44] A.D. Becke, J. Chem. Phys. 98 (7) (1993) 5648–5652.
- [45] P.J. Stephens, F.J. Devlin, C.F. Chabalowski, M.J. Frisch, J. Phys. Chem. 98 (45) (1994) 11623–11627.
- [46] A.D. Becke, Phys. Rev. A 38 (6) (1988) 3098–3100.
- [47] C.T. Lee, W.T. Yang, R.G. Parr, Phys. Rev. B 37 (2) (1988) 785–789.

- [48] R.D. Adamson, P.M.W. Gill, J.A. Pople, *Chem. Phys. Lett.* 284 (1–2) (1998) 6–11.
- [49] F.A. Hamprecht, A.J. Cohen, D.J. Tozer, N.C. Handy, *J. Chem. Phys.* 109 (15) (1998) 6264–6271.
- [50] P.J. Wilson, T.J. Bradley, D.J. Tozer, *J. Chem. Phys.* 115 (20) (2001) 9233–9242.
- [51] J.X. Yang, B.R. N'Guessan, A. Dedieu, D.C. Grills, X.Z. Sun, M.W. George, *Organometallics* 28 (11) (2009) 3113–3122.
- [52] X.Z. Sun, S.M. Nikiforov, J.X. Yang, C.S. Colley, M.W. George, *Appl. Spectrosc.* 56 (1) (2002) 31–39.
- [53] G.M. Greetham, P. Burgos, Q. Cao, I.P. Clark, P.S. Codd, R.C. Farrow, M.W. George, M. Kogimtzis, P. Matousek, A.W. Parker, M.R. Pollard, D.A. Robinson, Z.-J. Xin, M. Towrie, *Appl. Spectrosc.* 64 (12) (2010) 1311–1319.
- [54] Y. Shao, L.F. Molnar, Y. Jung, J. Kussmann, C. Ochsenfeld, S.T. Brown, A.T.B. Gilbert, L.V. Slipchenko, S.V. Levchenko, D.P. O'Neill, R.A. DiStasio Jr., R.C. Lochan, T. Wang, G.J.O. Beran, N.A. Besley, J.M. Herbert, C.Y. Lin, T. Van Voorhis, S.H. Chien, A. Sodt, R.P. Steele, V.A. Rassolov, P.E. Maslen, P.P. Korambath, R.D. Adamson, B. Austin, J. Baker, E.F.C. Byrd, H. Dachsel, R.J. Doerksen, A. Dreuw, B. D. Dunietz, A.D. Dutoi, T.R. Furlani, S.R. Gwaltney, A. Heyden, S. Hirata, C.-P. Hsu, G. Kedziora, R.Z. Khalliulin, P. Klunzinger, A.M. Lee, M.S. Lee, W. Liang, I. Lotan, N. Nair, B. Peters, E.I. Proynov, P.A. Pieniazek, Y.M. Rhee, J. Ritchie, E. Rosta, C.D. Sherrill, A.C. Simmonett, J.E. Subotnik, H.L. Woodcock III, W. Zhang, A.T. Bell, A.K. Chakraborty, D.M. Chipman, F.J. Keil, A. Warshel, W.J. Hehre, H.F. Schaefer III, J. Kong, A.I. Krylov, P.M.W. Gill, M. Head-Gordon, *Phys. Chem. Chem. Phys.* 8 (27) (2006) 3172–3191.
- [55] A.T.B. Gilbert, N.A. Besley, P.M.W. Gill, *J. Phys. Chem. A* 112 (50) (2008) 13164–13171.
- [56] W. Humphrey, A. Dalke, K. Schulten, *J. Mol. Graphics* 14 (1) (1996) 33–38.
- [57] M.J. van der Burgt, A.H. Huizer, C.A.G.O. Varma, B.D. Wagner, J. Lustzyk, *Chemical Physics* 196 (1–2) (1995) 193–210.
- [58] Y. Liu, J. Ding, R. Liu, D. Shi, J. Sun, *J. Comput. Chem.* 30 (16) (2009) 2723–2727.
- [59] S. Tanaka, C. Kato, K. Horie, H.-O. Hamaguchi, *Chem. Phys. Lett.* 381 (3–4) (2003) 385–391.
- [60] L.J. Andrews, A. Deroulede, H. Linschitz, *J. Phys. Chem.* 82 (21) (1978) 2304–2309.

Figure captions

Fig. 1. (i) Calculated harmonic EDF1 IR spectra and (ii) FT-IR spectra in scKr. (a) 2-naphthaldehyde, (b) 9-fluorenone.

Fig. 2. MAD values for 2-naphthaldehyde, comparing the calculated harmonic and experimental frequencies with the CO stretching mode included (dark), and excluded (light).

Fig. 3. MAD values for 9-fluorenone, comparing the calculated harmonic and experimental frequencies with the CO stretching mode included (dark), and excluded (light).

Fig. 4. IR spectra of 2-naphthaldehyde. (i) and (iii) IR spectra of the T_1 state, measured in CD_3CN 100 ns after photoexcitation and in scKr 1 μs after photoexcitation at 355 nm. (ii) and (iv) FT-IR spectra measured in CD_3CN and scKr. (v) the calculated (B97-1/6-311G(d,p), scaled harmonic) spectrum of the T_1 state.

Fig. 5. IR spectra of 2-naphthaldehyde. (i) the IR spectrum of the S_1 state, measured in CD_3CN 0.1 ns after photoexcitation. (ii) the FT-IR spectrum measured in CD_3CN . (ii) the calculated (B97-1/6-311G(d,p), scaled harmonic) spectrum of the S_1 state.

Fig. 6. Kinetic trace of the bands of the 2-naphthaldehyde S_1 state decaying, concomitant with growth of the T_1 state ($s = 9 \pm 4$ ns). The initial rise of the S_1 state band occurs again, this time the S_1 state bands arise from a nearly featureless spectrum ($s = 6 \pm 2$ ps) that consists only of bleaches.

Fig. 7. IR spectra of 9-fluorenone. (i) and (iii) IR spectra of the T_1 state, measured in CD_3CN 100 ns after photoexcitation and in scKr 1 μs after photoexcitation at 355 nm. (ii) and (iv) FT-IR spectra measured in CD_3CN and scKr. (v) the calculated (B97-1/6-311G(d,p), scaled harmonic) spectrum of the T_1 state.

Fig. 8. IR spectra of 9-fluorenone. (i) the IR spectrum of the S_1 state, measured in CD_3CN 0.1 ns after photoexcitation. (ii) the FT-IR spectrum measured in CD_3CN . (ii) the calculated (B97-1/6-311G(d,p), scaled harmonic) spectrum of the S_1 state.

Fig. 9. Kinetic trace of the bands of the 9-fluorenone S_1 state decaying, concomitant with growth of the T_1 state ($s = 7 \pm 1$ ns). The initial rise of the S_1 state band ($s = 10 \pm 2$ ps) is manifested in the spectra as a slight blueshift of the bands and may be due to internal conversion or cooling.

Fig. 10. The (a) HOMO-1, (b) HOMO, and (c) LUMO orbitals of 2-naphthaldehyde.

Fig. 11. The (a) HOMO-1, (b) HOMO, and (c) LUMO orbitals of 9-fluorenone.

Fig. 12. MAD values for 2-naphthaldehyde, comparing the calculated anharmonic and experimental frequencies with the CO stretching mode included (dark), and excluded (light).

Fig. 13. MAD values for 9-fluorenone, comparing the calculated anharmonic and experimental frequencies with the CO stretching mode included (dark), and excluded (light).

Table captions

Table 1. Experimentally prominent IR modes of the S_0 state of 2-naphthaldehyde. Unscaled harmonic frequencies shown. Calculated differences from scKr (expt) are shown in parentheses.

Table 2. Experimentally prominent IR modes of the S_0 state of 9-fluorenone. Unscaled harmonic frequencies shown. Calculated differences from scKr (expt) are shown in parentheses.

Table 3. Experimentally prominent IR modes of the T_1 and S_1 states of 2-naphthaldehyde, shown for experiment and calculated scaled harmonic spectra. Calculated differences from experiment are shown in parentheses.

Table 4. Experimentally prominent IR modes of the T_1 and S_1 states of 9-fluorenone, shown for experiment and calculated scaled harmonic spectra. Calculated differences from experiment are shown in parentheses.

Table 5. Experimentally prominent IR modes of the T_1 state of 2-naphthaldehyde. Calculated differences from scKr (expt) are shown in parentheses.

Table 6. Experimentally prominent IR modes of the T_1 state of 9-fluorenone. Calculated differences from scKr (expt) are shown in parentheses.

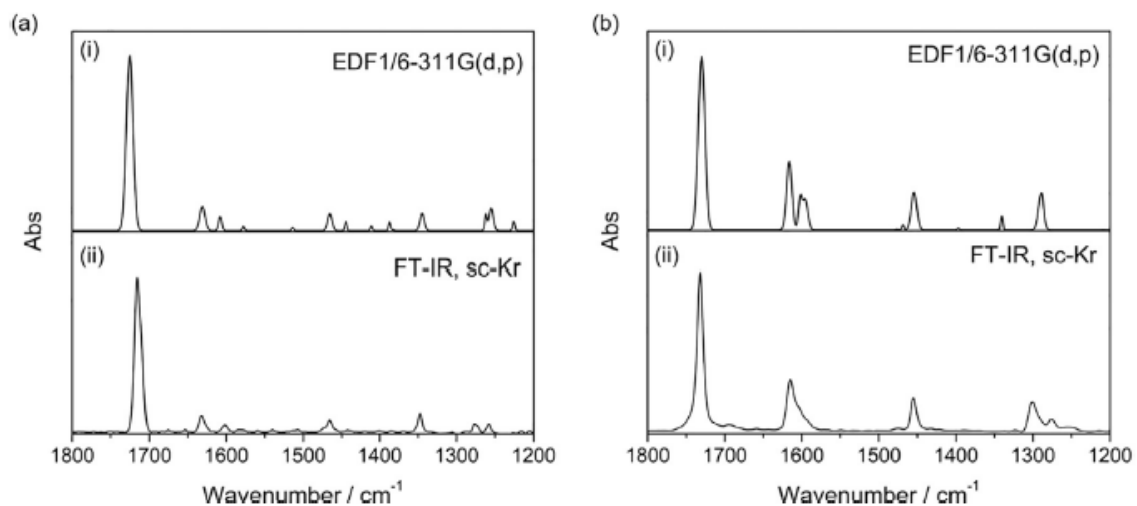


Fig. 1.

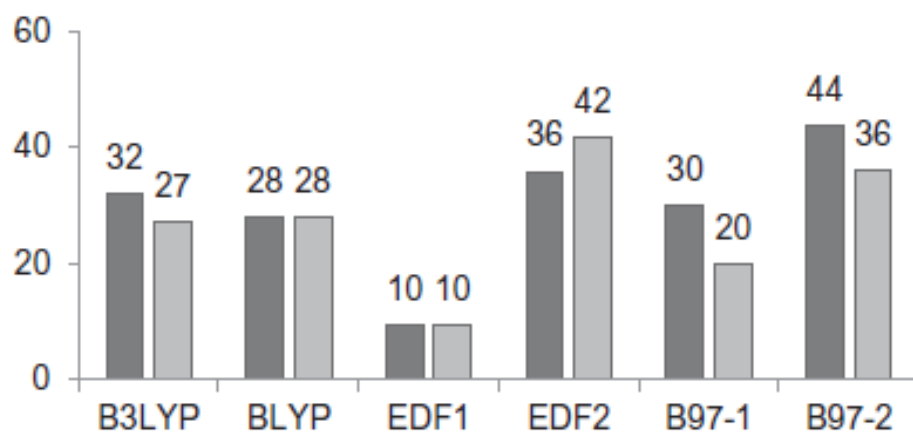


Fig. 2.

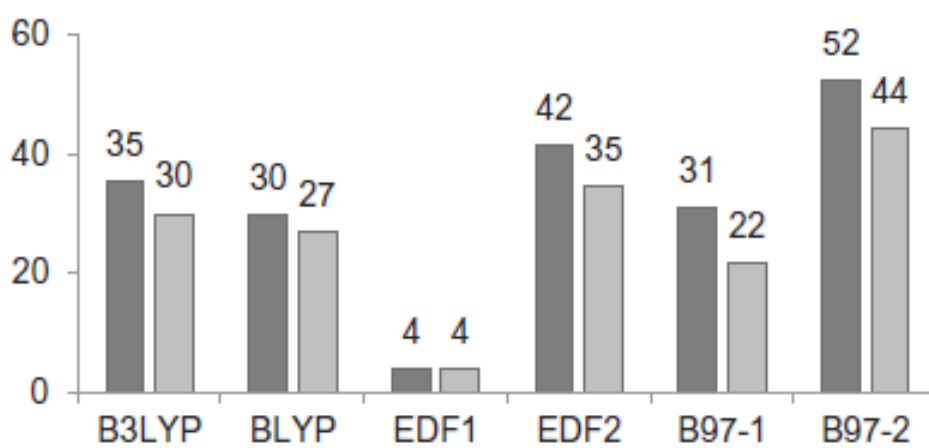


Fig. 3.

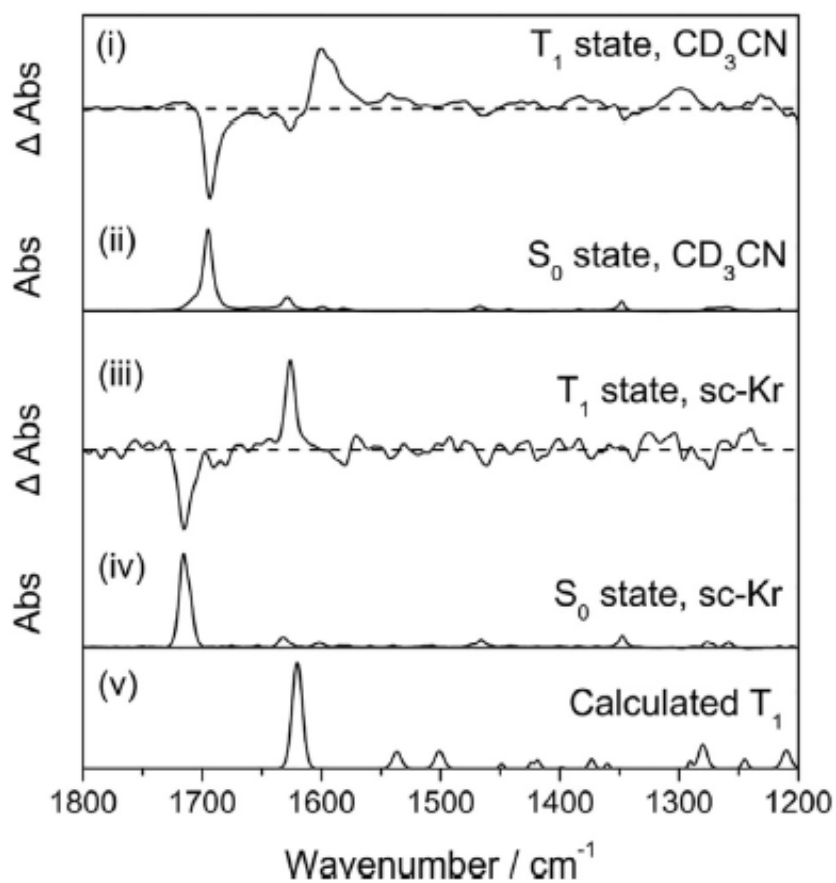


Fig. 4.

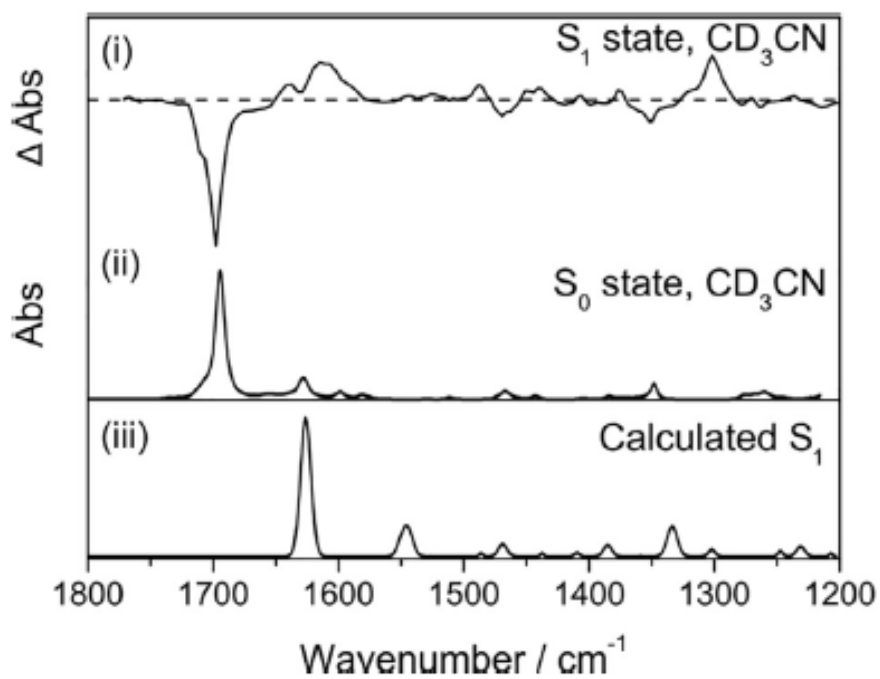


Fig. 5.

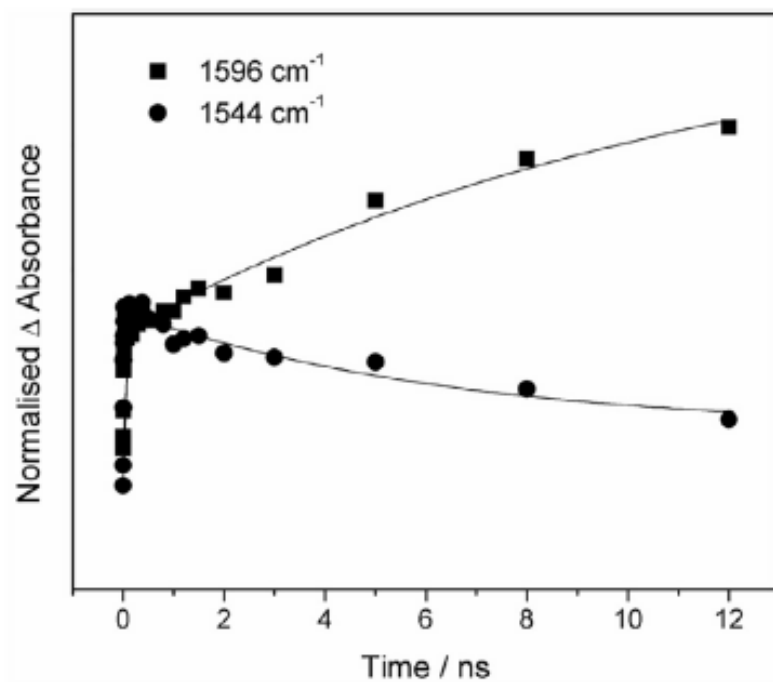


Fig. 6.

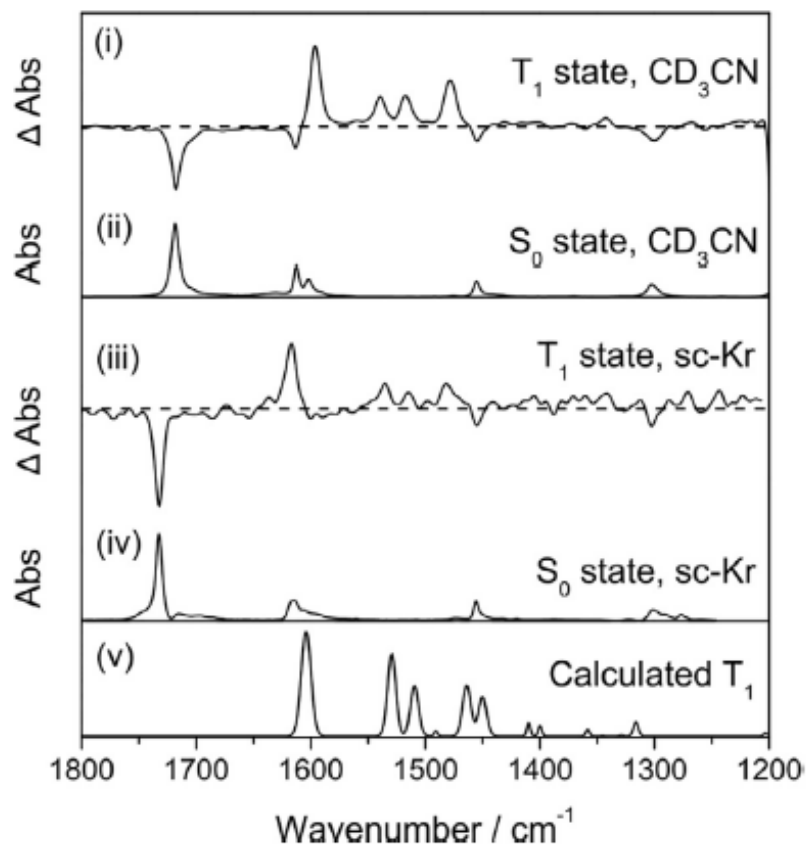


Fig. 7.

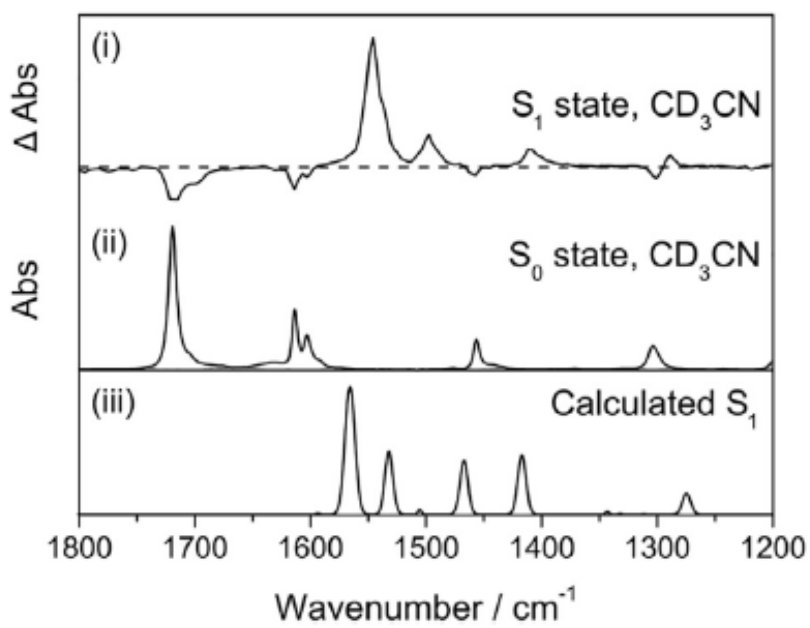


Fig. 8.

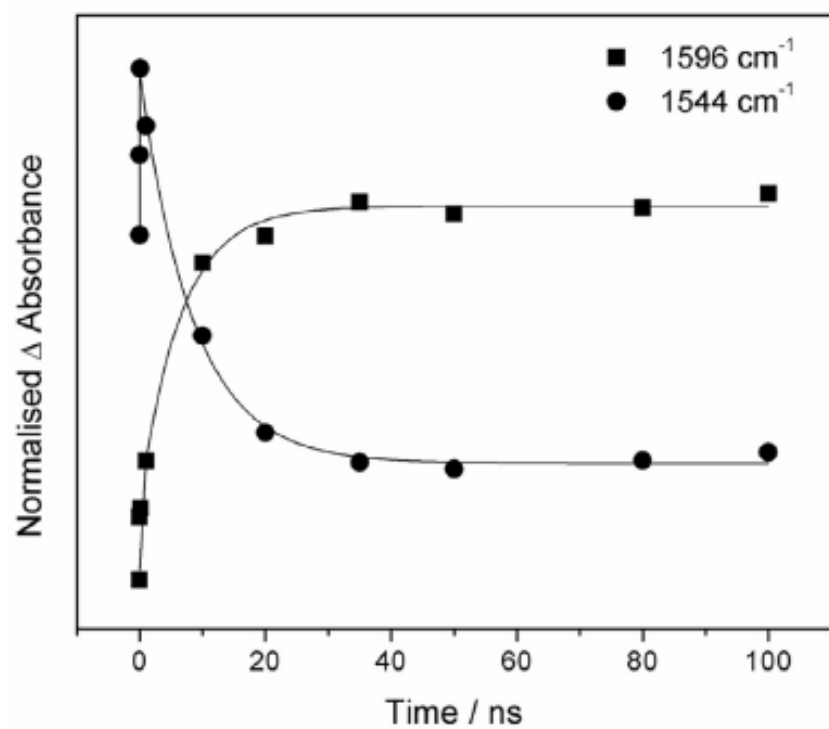


Fig. 9.

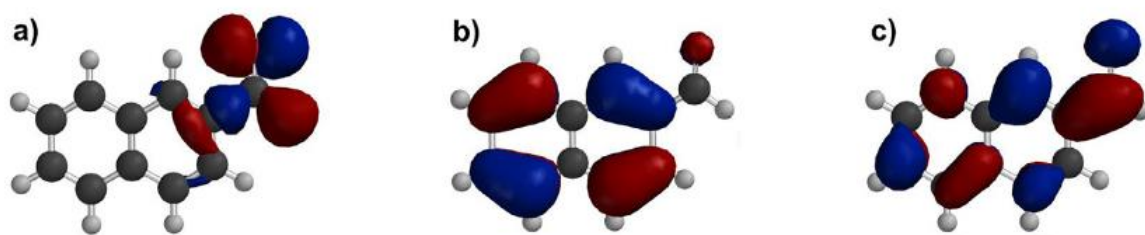


Fig. 10.

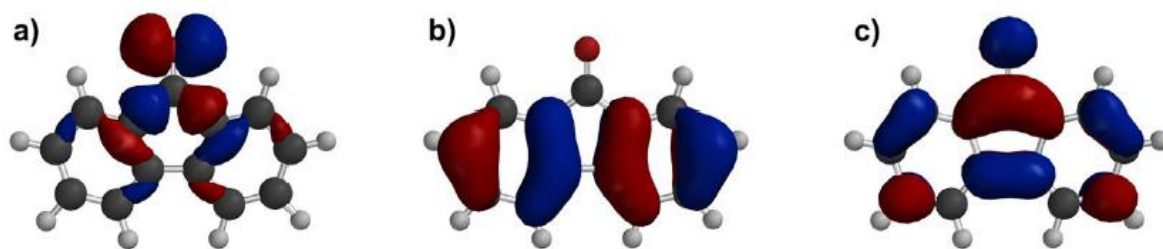


Fig. 11.

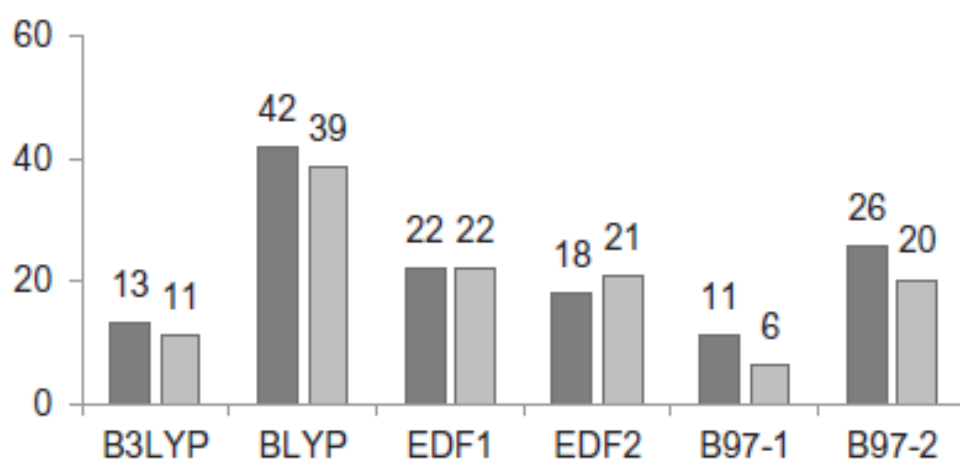


Fig. 12.

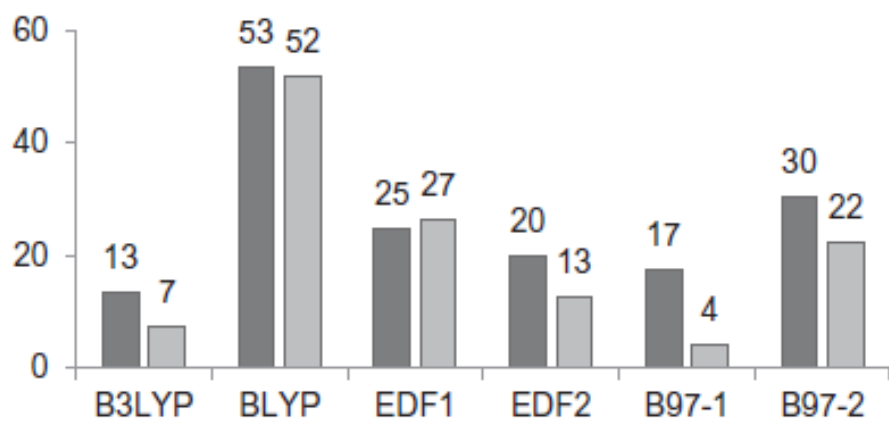


Fig. 13.

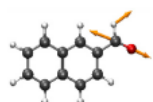
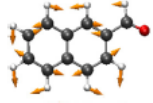
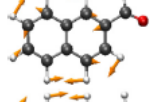
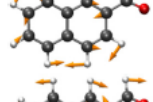
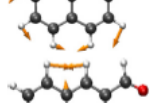
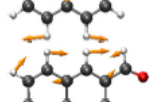
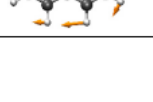
Mode	CD ₃ CN (expt)	Band positions/cm ⁻¹			B97-1 TOSH	Visualisation
		scKr (expt)	EDF1 harm.	B97-1 harm.		
ν_{46}	1696	1715	1725 (10)	1787 (72)	1748 (33)	
ν_{45}	1628	1632	1631 (-1)	1663 (31)	1642 (10)	
ν_{44}	1599	1602	1608 (6)	1637 (35)	1614 (12)	
ν_{41}	1468	1466	1466 (0)	1491 (25)	1474 (8)	
ν_{36}	1348	1348	1345 (-3)	1367 (19)	1349 (1)	
ν_{35}	1274	1277	1262 (-15)	1282 (5)	1270 (-7)	
ν_{34}	1259	1258	1226 (-32)	1235 (-23)	1265 (7)	

Table 1.

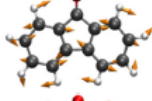
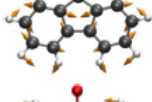
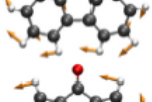
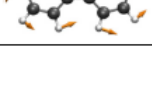
Mode	CD ₃ CN (expt)	Band positions/cm ⁻¹				Visualisation
		scKr (expt)	EDF1 harm.	B97-1 harm.	B97-1 TOSH	
ν_{52}	1718	1732	1730 (-2)	1799 (67)	1800 (68)	
ν_{51}	1612	1615	1616 (1)	1645 (30)	1623 (8)	
ν_{50}	1602	1606	1602 (-4)	1632 (26)	1611 (5)	
ν_{45}	1456	1455	1454 (-1)	1477 (22)	1460 (5)	
ν_{41}	1302	1301	1289 (-12)	1311 (10)	1300 (-1)	

Table 2.

Mode	Band positions/cm ⁻¹		Mode	Band positions/cm ⁻¹	
	CD ₃ CN T ₁ (expt)	B97-1T ₁ Scaled		CD ₃ CN S ₁ (expt)	B97-1 S ₁ Scaled
ν_{46}	1600	1620 (20)	ν_{46}	1638	1626 (-12)
-	1591	-	-	1613	-
ν_{45}	1543	1536 (-7)	ν_{41}	1487	1468 (-19)
ν_{44}	1526	1501 (-25)	ν_{40}	1439	1437 (-2)
ν_{36}	1299	1279 (-20)	ν_{38}	1375	1384 (-9)
			ν_{36}	1300	1332 (32)

Table 3.

Mode	Band positions / cm^{-1}		Mode	Band positions / cm^{-1}	
	CD ₃ CN T ₁ (expt)	B97-1T ₁ Scaled		CD ₃ CN S ₁ (expt)	B97-1 S ₁ Scaled
ν_{52}	1596	1603 (7)	ν_{51}	1545	1565 (20)
ν_{51}	1539	1528 (-11)	ν_{49}	1496	1531 (35)
ν_{50}	1517	1508 (-9)	ν_{44}	1409	1417 (8)
$\nu_{48/47}$	1477	1463/1449	ν_{40}	1278	1275 (-3)
ν_{46}	1430	1409 (-21)			
ν_{41}	1342	1315 (-27)			

Table 4.

Mode	Band positions/ cm^{-1}		
	CD ₃ CN (expt)	scKr (expt)	B97-1 TOSH
ν_{46}	1600	1626	1628 (2)
–	1591	–	–
ν_{45}	1543	1570	1556 (-14)
ν_{44}	1526	1558	1513 (-42)
ν_{36}	1299	1304	1315 (10)

Table 5.

Mode	Band positions/cm ⁻¹		
	CD ₃ CN (expt)	scKr (expt)	B97-1 TOSH
ν_{52}	1596	1617	1619 (2)
ν_{51}	1539	1535	1548 (13)
ν_{50}	1517	1514	1523 (9)
$\nu_{48/47}$	1477	1491/1482	1483 (-8)/1477 (-5)
ν_{46}	1430	1442	1436 (-6)
ν_{41}	1342	1342	1344 (2)

Table 6.